

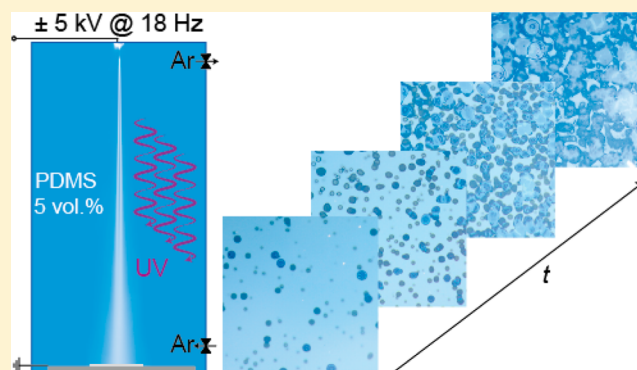
Thin Film Formation and Morphology of Electrospayed Polydimethylsiloxane

Florian M. Weiss,^{†,‡} Tino Töpfer,[†] Bekim Osmani,[†] Hans Deyhle,[†] Gabor Kovacs,[‡] and Bert Müller^{*,†}

[†]Biomaterials Science Center, Department of Biomedical Engineering, University of Basel, Gewerbestrasse 14, 4123 Allschwil, Switzerland

[‡]Federal Laboratories for Materials Science and Technology, Überlandstrasse 129, 8600 Dübendorf, Switzerland

ABSTRACT: Low-voltage dielectric actuators (DEAs) can be fabricated using submicrometer-thin polydimethylsiloxane (PDMS) films. The two established techniques, namely spin coating and molecular beam deposition, however, are inappropriate to produce multistack DEAs in an efficient way. Therefore, we propose an alternative deposition technique, i.e., the alternating current electrospay deposition (ACESD) of 5 vol % PDMS in ethyl acetate solution and subsequent ultraviolet light curing. Atomic force microscopy makes possible the three-dimensional analysis of cured droplet-like islands. These circular islands, prepared on 2 in. Si(100) wafers from four polymers with molecular masses between 800 and 62 700 g/mol, reveal a characteristic morphology with an increasing height-to-diameter ratio. Using the 6000 g/mol polymer for ACESD, the film morphology evolution was tracked by applying conventional optical microscopy and spectroscopic ellipsometry. When the deposition was terminated after 13 s, circular islands with a mean height of 30 nm were found, while terminating the deposition after about 155 s led to a confluent layer with a mean height of 91 ± 10 nm. Potential electrostatic interactions between the droplets could not be identified through the analysis of spatial island distribution. Nevertheless, ACESD is a budget-priced and competitive deposition technique that can be employed to fabricate submicrometer-thin PDMS films with true nanometer roughness.



1. INTRODUCTION

Molecular beams enable the formation of organic thin films with monolayer precision, as required for applications in (opto)electronics.¹ These flexible but rather expensive deposition techniques are limited to comparably small molecules. Organic molecule deposition is a growing field, although a variety of materials cannot be evaporated because of their limited thermal stability.² Furthermore, the deposition rates are restricted to less than one monolayer per second, which corresponds to about one micrometer per hour. For example, the fabrication of a stacked dielectric elastomer actuator (DEA) requires about 10 000 h to reach a thickness of several millimeters. This simple estimation shows that alternative methods have to be identified, for example, to fabricate low-voltage DEAs.

Currently, DEAs, which find their application in robotics,^{3,4} haptics,⁵ lens systems,^{6,7} sound generation systems,⁸ and sensors,^{9,10} are built from elastomers purchased as films from well-established suppliers or prepared using spin-coating. These elastomer films are thicker than one micrometer and hence require operation voltages of several hundred volts to reach strains of about 10%. As the operation voltage of a DEA increases with the square of the elastomer thickness, even a moderate thickness reduction by less than 1 order of magnitude

is an essential step toward low-voltage DEAs as required for medical implants, including artificial muscles.¹¹ In this paper, we pursue electrospaying to fabricate nanometer-thin silicone films. The application of a static electric field for the electrospaying process, however, may be problematic because the charges will accumulate on the isolating substrate. To avoid substrate charging, we propose to employ an alternating current (ac) source.

At first glance, one might expect a film morphology that represents the arbitrary droplet-by-droplet deposition, i.e., a rough film surface. Nonetheless, since the spray droplets not only contain the polymers but also consist mainly of the wetting solvent, one can reasonably expect flat islands with a high aspect ratio between diameter and height. With a PDMS–solvent ratio of 1:20, droplet difflence on the Si(100) wafer, and the coalescence of islands, we may reasonably expect the formation of a homogeneous, confluent layer. Because of the evaporation of the solvent at a moderate rate, and energy input via ultraviolet light curing, nanometer-thin silicone films with a uniform thickness and low surface roughness might be created.

Received: February 6, 2016

Revised: March 14, 2016

Published: March 15, 2016

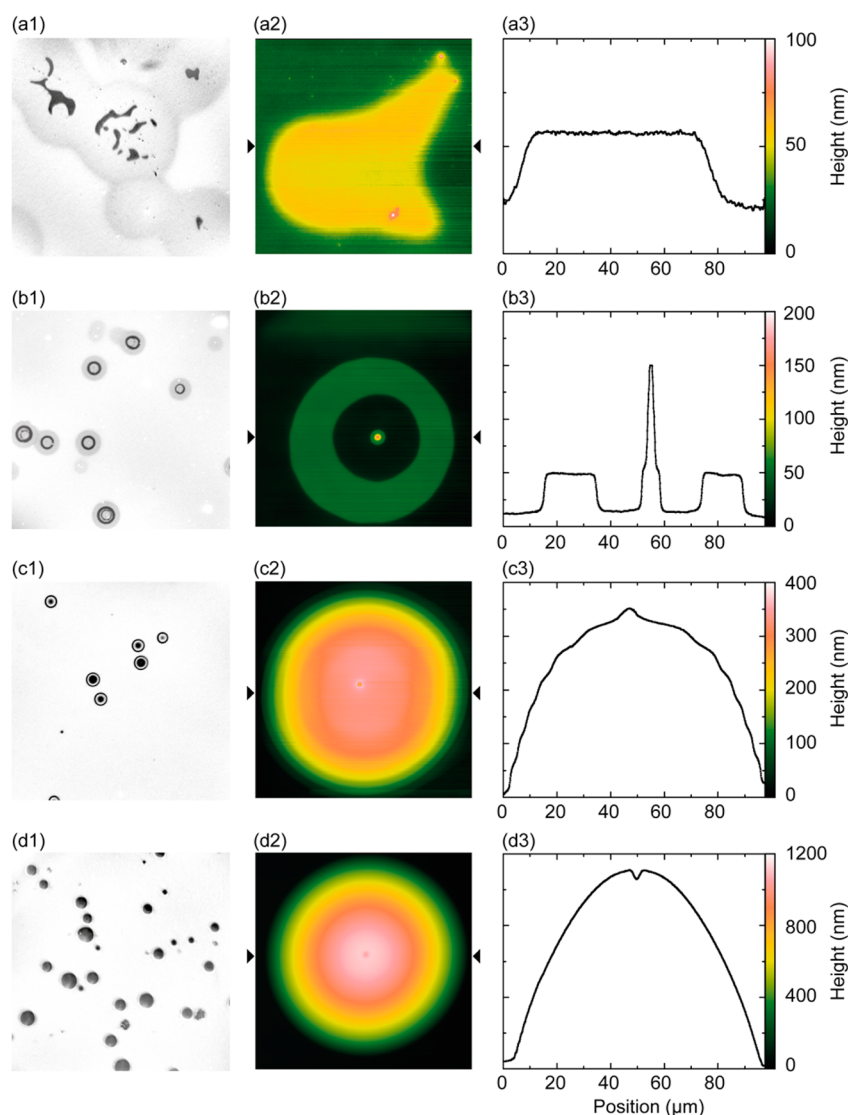


Figure 1. Characteristic morphology of UV-cured PDMS islands electrospayed at a flow rate of 267 nL/s by applying a voltage of ± 5 kV and a frequency of 18 Hz, revealed by means of (1) optical microscopy, image size: 2.34 mm \times 2.34 mm; (2) AFM images, size: 97.5 μm \times 97.5 μm ; and (3) AFM profiles with locations indicated by the arrow heads. The polymer chain lengths correspond to number-average molecular weights of (a) 800, (b) 6000, (c) 28 000, and (d) 62 700 g/mol.

Homogeneity may even be enhanced, since the process includes the charging of the droplets, which in turn leads to repulsive electrostatic interactions between them.

We hypothesize that the choice of polymer size determines the islands' height-to diameter ratio, as their mobility depends on molecular mass.¹² Atomic force microscopy (AFM) is perfectly suited for measuring surface morphology and is especially sensitive for island heights. Thus, AFM studies will assist in the search for the optimized size of PDMS molecules to be deposited.

Once the polymer size has been selected, the evolution of film morphology with the advancement of deposition from the early stages of deposition, i.e., the formation of individual islands, to the advanced stages of film growth, i.e., the development of a confluent layer, should be investigated. The spatial distribution of the individual islands can be derived from optical micrographs. Here, island distribution will shed light on the interactions between the charged droplets during and after deposition. This analysis, however, becomes challenging when the individual islands merge and form a confluent layer.

Therefore, for the advanced stages of film growth, we propose characterizing the film by means of spectroscopic ellipsometry, which reveals the wavelength-dependent refractive index, film thickness, surface morphology, and film porosity.¹³

The application of these characterization techniques and the related analysis of the experimental data allow for the enhancement of the electrospaying process for elastomer thin films that can be exploited for low-voltage DEA nanostructures.

2. EXPERIMENTAL SECTION

2.1. Material and Electrospay Deposition. Vinyl-terminated PDMS polymers (Gelest, USA) with number-average molecular weights M_n of 800, 6000, 28 000, and 62 700 g/mol (DMS-V05, DMS-V21, DMS-V31, and DMS-V41, respectively) were dissolved in ethyl acetate (Laboratory reagent grade, Fisher Scientific UK, Brunschwig, Basel, Switzerland) to obtain the 5 vol % solution. PDMS samples and solvent were used as purchased. The polymer solution was then drawn up into a 3 mL glass syringe with a metallic Leur-lock (Eternal-Matic, Sanitex, HUBERLAB, Aesch, Switzerland) and connected to a metallic nozzle (26s, Hamilton, Bonaduz,

Switzerland) with an inner diameter of 0.13 mm. The flow rate of the syringe pump (Aladdin six-syringe pump, World Precision Instruments Germany GmbH, Berlin, Germany) was set to 267 nL/s. The applied voltage on the nozzle originates from a voltage source (TREK, 5/80, Lockport, NY). It is coupled with a function generator (Model 119M, Max Meier Elektronik, Zurich, Switzerland) in order to apply a rectangular voltage function of ± 5 kV with a frequency of 18 Hz, monitored by a Tektronix oscilloscope (TDS 210, Computer Control AG, Zurich, Switzerland). A distance of 67 mm from the Si substrate (SiMat, Silicon Materials, Kaufering, Germany) to the nozzle was chosen. UV-curing was performed without any photoinitiator in an Ar (Carbagas AG, Basel, Switzerland) atmosphere of 1 bar, applying UV radiation from a deuterium broad-band UV lamp (Yuyu Lightning, China) and covering a spectral range between 180 and 450 nm, with its maximum intensity at a wavelength of 210 nm at a distance of 2 cm.

2.2. Atomic Force Microscopy. AFM measurements ($97.5 \times 97.5 \mu\text{m}^2$, tapping mode, vibration amplitude 3000 mV, set point 35%) were performed using a FlexAFM system (Nanosurf AG, Liestal, Switzerland). Using a noncontact soft tapping AFM probe (PPP-NCSTR-10 probe, tip height 10–15 μm , force constant 1.2–29 N/m, NANOSENSORS, Neuchatel, Switzerland), 512 lines at a speed of 5.08 s per line were acquired for the image. The raw data were leveled removing a second-degree polynomial background. Root-mean-square values were calculated using the Gwyddion 2.41 software package (Gwyddion: an open-source software for SPM data analysis, <http://gwyddion.net>).¹⁴

2.3. Optical Micrographs. Images of the PDMS islands and layers at preselected deposition periods after curing were taken with a Canon EOS 600D camera mounted on a Stemi DV4 SPOT microscope (Carl Zeiss AG, Feldbach, Switzerland) with a magnification of 13.

2.4. Island Segmentation. The acquired color images were converted to grayscale using MATLAB (The MathWorks, Inc., Natick, United States). To account for inhomogeneous illumination, the images were leveled by means of second-degree polynomial background subtraction. A 2D Frangi filter implemented in MATLAB (The MathWorks, Inc., Natick, United States)¹⁵ was used to identify the borders of the PDMS islands. The borders' open ends were closed manually in order to generate a binary mask representing the segmented PDMS islands on the Si(100) substrate.

2.5. Spectroscopic Ellipsometry. The SE801 spectroscopic ellipsometer from SENTECH (Berlin, Germany), controlled by SpectraRay3 software, was applied after deposition and curing. As a function of the wavelength between 190 and 1050 nm, angles Ψ and Δ were measured. The Fresnel equation

$$\rho = r_p/r_s = \tan \Psi e^{i\Delta}$$

provides the relation between the recorded Ψ and Δ data and the complex Fresnel reflection coefficients r_p and r_s of p- and s-polarized light and their ratio ρ . This approach helps extract the wavelength-dependent dielectric function $\tilde{n}(\lambda)$

$$\langle \tilde{n} \rangle^2 = (\langle n \rangle + i\langle k \rangle)^2 = \sin(\phi_0)^2 \left(1 + \tan(\phi_0)^2 \left(\frac{1 - \rho}{1 + \rho} \right)^2 \right)$$

with ϕ_0 being the angle of the incident beam and $n(\lambda)$ the real and $k(\lambda)$ the complex parts of the refractive index. The incident beam with a diameter of 4 mm and an angle of incidence of $\phi_0 = 70^\circ$ from the normal results in a measured area of 4 mm \times 10 mm on the Si(100) wafer. During the step scan mode eight polarizer positions with fixed integration times of 0.1 s were monitored. To determine the linear and first-order nonlinear refractive index of the cured DMS-V21, a spin-coated, 2 μm thick film was measured. The analysis provided $n_0 = 1.396 \pm 0.005$, $n_1 = 30.0 \pm 0.7$, and $n_2 = 7.0 \pm 0.2$. These values are based on the Cauchy series approximation¹⁶ with the refractive index $n(\lambda) = n_0 + c_1 n_1/\lambda^2 + c_2 n_2/\lambda^4$ with $c_1 = 10^2 \text{ nm}^2$ and $c_2 = 10^4 \text{ nm}^2$. The extinction coefficient k was set to zero.

3. RESULTS AND DISCUSSION

3.1. Selection of the Polymer Chain Length. In order to find an optimized starting material size or polymer length for the formation of nanometer-thin elastomer films, the morphology of four ac electrospayed PDMS islands were investigated after UV curing. The characteristic morphology is recognized in optical micrographs, as displayed in Figure 1, panels (a1), (b1), (c1), and (d1). The vinyl-terminated PDMS islands, prepared using polymers with molecular weights of 800 and 6000 g/mol, DMS-V05 and DMS-V21, exhibit a shape that reflects the spreading out of the sprayed droplets, as indicated in the optical micrographs of Figure 1, panels (a1) and (b1), by the light-gray area with the darker rings. The diameter of the PDMS islands shrinks with increasing molecular weight. For islands prepared from the polymers with the higher molecular weight, i.e., 28 000 and 62 700 g/mol, DMS-V31 and DMS-V41, no ring could be identified, as illustrated in Figure 1, panels (c1) and (d1). Compared to optical micrographs the AFM images comprise only a restricted area, but they do provide a precise measure of the islands' heights. Furthermore, the islands' shapes are characteristic for each polymer. Those electrospayed using DMS-V05 have plateau-like features about 30 nm high with an aspect ratio of width-to-height of 2700 (cf. Figure 1, panels (a1)–(a3)). PDMS islands fabricated from DMS-V21 show rings that are also about 30 nm high, and these rings enclose an island. Although the profile in Figure 1(b3) presents a rather sharp peak, this island has a height that is 3 orders of magnitude smaller than its diameter. Islands electrospayed using DMS-V31 also show the rings on the optical micrographs (Figure 1(c1)). However, when investigating them by AFM, steps of about 50 nm in height, concentrically arranged around their center, are found, as best recognized in Figure 1(c3). Islands prepared from the polymer DMS-V41 do not show steps. They increase from the periphery to the center, as given in Figure 1, panels (d1)–(d3). In the center, one finds a notch. The diameter-to-height ratio of the islands corresponds to about 900.

The characteristic morphology of the PDMS islands prepared by electrospaying and subsequent UV curing is not fully understood. Nevertheless, there are several publications that describe selected phenomena related to island formation. For example, Grishaev et al.¹⁷ very recently published a study on the complex drop impact morphology of a series of millimeter-size droplets onto hydrophobic and hydrophilic substrates. The present study, however, restricts its focus to the ethyl acetate solvent and the Si(100) substrate. This means that only the 5 vol % polymer caused the characteristic differences seen in the PDMS island shapes. The chain length of the polymers seems to determine diffluence, which is significantly higher for the low-molecular-weight polymers. It can be reasonably stated that the starting materials from Gelest contain oligomers and residuals from the polymerization process, which may influence the wetting behavior. Furthermore, one can assume that 5.0 vol % is well below the overlap concentration of the used polymers. Entanglement effects, which definitely influence the film morphology on nanometer scale, however, become important for the spray on the route from nozzle to substrate because a significant amount of solvent evaporates.

Because the UV radiation treatment changes the morphology and the mechanical properties of the sprayed liquid PDMS film,¹⁸ one may expect that the UV light induces cross-linking.

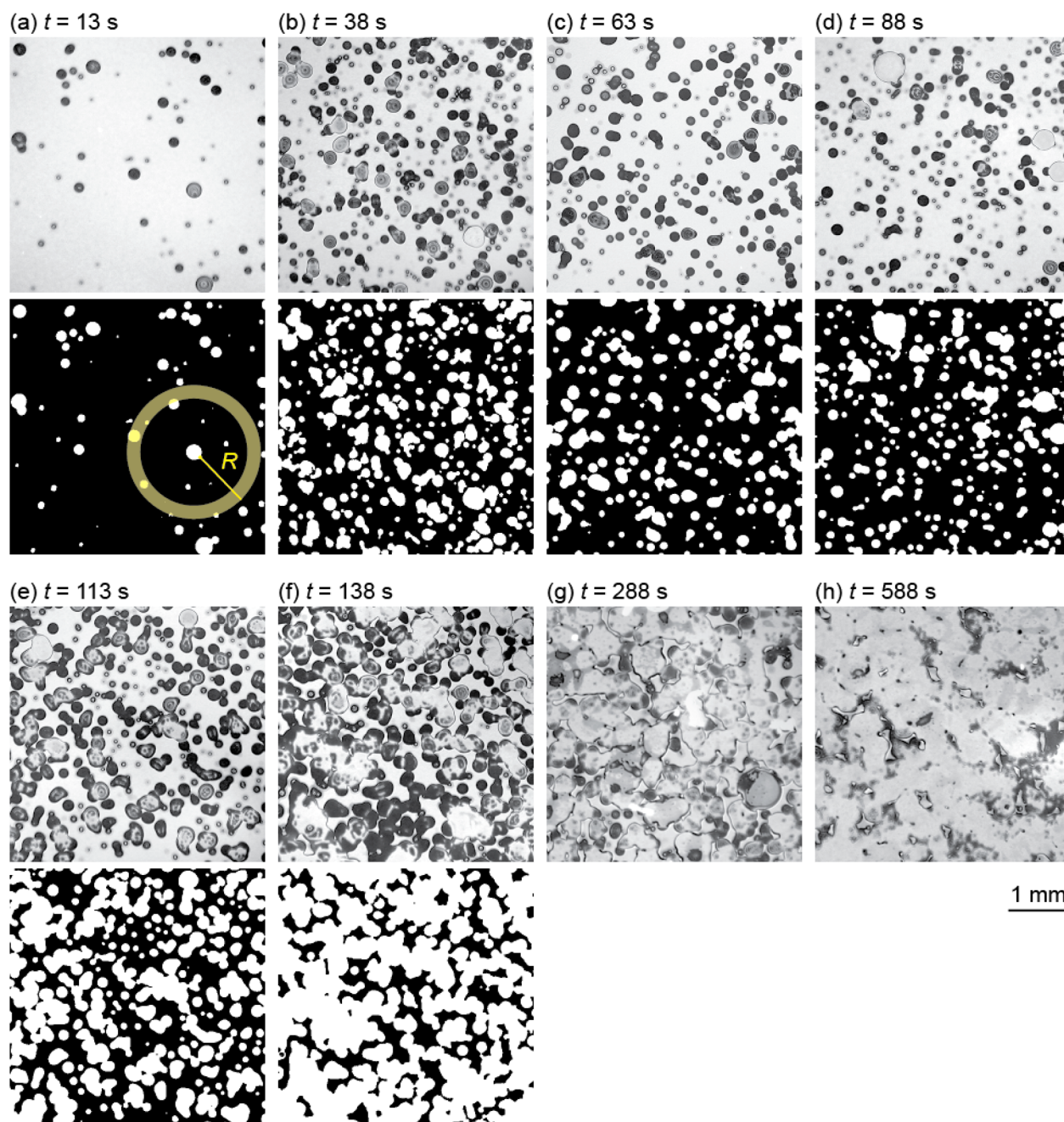


Figure 2. Optical micrographs of electrospayed and cured PDMS on Si(100). Deposition time t is indicated. The segmentation of the PDMS islands, white on the black substrate on the images below the micrographs, allows for defining the coverage and analyzing island separation. The yellow scheme in mask (a) elucidates the definition of the radial coverage θ_R . The distance R from each island periphery is calculated according to the distance transform. The radial coverage θ_R for a given R is obtained as the ratio white to black and white at distance R (cf. yellow shaded area). The procedure is repeated for each individual island, and the results are averaged.

The reaction mechanism is associated with a reduced concentration of vinyl functional groups as shown by IR spectroscopy.¹¹ Furthermore, the investigation of UV-irradiated PDMS using wavelengths of about 170 nm revealed scissions of the Si-CH₃ and -CH₂-H bonds.¹⁹ Therefore, a cross-linking mechanism based on the radicalization of these three bonds could lead to a three-dimensional elastomer network.

Contrary to the plateaus, the rings perfectly represented in Figure 1, panels (b1) and (b2), were described two decades ago.²⁰ In the work of Deegan and co-workers, it is explained that once the contact line of an emulsion or a colloidal suspension is pinned to the substrate, the rim of the ring forms.

Solute particles are too large to migrate further in the surrounding solvent, and capillary force drags the solvent toward the contact line, because here the solvent evaporates preferentially. Thus, one may conclude that the more solute molecules in a droplet, the broader the resulting ring. The rather flat island found in the center of the rings featuring an inclination of about 1.5° (cf. Figure 1, panels (b1)–(b3)) may occur as a result of curing, a process which may “freeze” the transport of the solute molecules toward the ring. Consequently, the remaining and mobile solute particles may build up into a heap, thus initiating transport toward the center—again driven by capillary forces due to preferential evaporation.

For the DMS-V31 and DMS-V41 polymers, one has to encounter the entanglement of the chains once they are deposited on substrate. At this stage the concentration of the polymer should have notably increased or even turned into the pure PDMS due to the solvent evaporation in the course of the spraying process. For PDMS the occurrence of entanglements is reported above a critical molecular weight between 10 100 and 12 500 g/mol.²¹

The concentric steps of the PDMS islands prepared from the polymer DMS-V31 resemble PDMS microdroplets described in the literature.²² Whereas the height of the steps reported in the literature corresponds to a few nanometers, we have identified step heights of several tens of nanometers which may originate from smectic ordering of the single polymer chains.²³

The phenomenon observed for DMS-V31, however, can also be explained through the capillary waves which propagate along the surface after the impact of the droplet, as described for water drops.²⁴ As the viscosity of the ethyl acetate solution with PDMS differs from that of water, the temporal evolution of the waves is probably modified. The nonoccurrence of steps on the semispherically shaped PDMS islands made from DMS-V41 droplets indicates that the capillary waves are suppressed because of the changed viscosity.

The notch on top of the PDMS islands prepared using DMS-V41 presumably originates from the droplet impact evolution just before the rebounding process of a secondary droplet starts. Here, viscosity slows down the process.

An investigation into the island morphology shows that DMS-V05 and DMS-V21 are better suited for preparing smooth nanometer-thin PDMS layers than the other two polymers used. Because the longer polymer chains build unimodal films with higher elasticity, DMS-V21 is preferred. Therefore, the present study concentrates on the usage of DMS-V21 dissolved in pure ethyl acetate.

3.2. From Islands to Confluent Film. Figure 2 depicts optical micrographs of PDMS on Si(100), each 4.24 mm × 4.24 mm, after deposition times t ranging from 13 to 588 s. For deposition times up to 90 s, the PDMS islands are well separated, as clearly displayed in the binary data below the optical micrographs. At higher coverage the islands coalesce. Therefore, PDMS films prepared with a deposition time longer than 150 s appear as a confluent layer.

The PDMS islands were automatically segmented to determine their coverage and to analyze island separation. The simultaneously performed manual segmentation validated the appropriate choice of threshold.

Coverage θ arises from the surface fraction covered by the PDMS islands, which is easily derived from the segmented data by dividing the number of pixels belonging to the PDMS by the total number of pixels in the image, as shown in Figure 2. These data are plotted as the function of the deposition time t in Figure 3. The linear fit through the point of origin underlines expected dependence. It should be noted that the entire deposition system had a delay time of about 12 s, which is readily obtained using the linear fit given in Figure 3.

The choice of coverage, however, is somewhat arbitrary. Hence, it makes sense to decode the deposition time by the means of the average film thickness d^* . In a previous study with the same setup, a deposition rate of 1.14 ± 0.06 nm/s was found for a flow rate of 267 nL/s.¹⁸

The diagram in Figure 4 displays mean radial coverage, determined as the distance from each segmented PDMS island surface. Around each island one finds a depletion zone with an

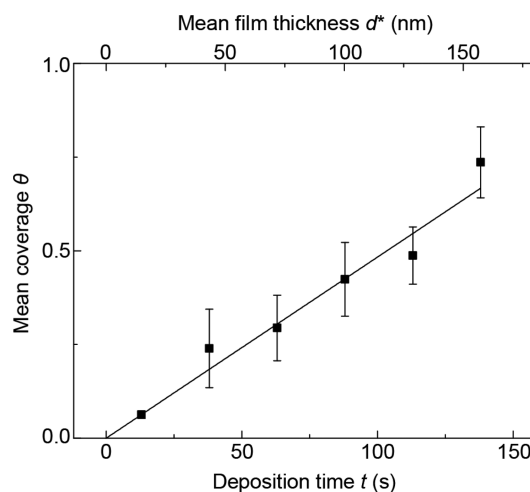


Figure 3. As expected, mean coverage θ is a linear function of deposition time t . Therefore, mean film thickness d^* is obtained from deposition time t via a deposition rate of 1.14 nm/s extracted in a previous study.¹⁸

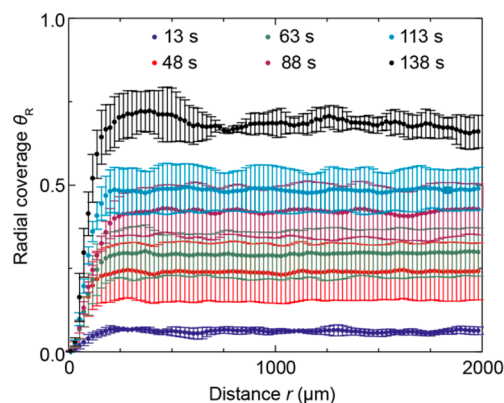


Figure 4. Mean radial coverage θ_R is plotted against the distance of the PDMS islands R . Here, for each segmented island (cf. Figure 2) coverage as a function of radial distance R was calculated. The procedure was repeated for each individual island in one micrograph. The diagram shows the average values of three optical micrographs. The error bars correspond to the related standard deviations.

extension of up to 250 μm , which is independent of deposition time. For larger radial distances, radial coverage reaches a deposition time-dependent plateau. These plateau values correspond to the mean coverage θ represented in Figure 3.

In order to better characterize the depletion zones, slope s is extracted from the data points represented in Figure 4. For this purpose, we use data points in the interval from 20 to 80% between zero and the plateau value of the mean radial coverage θ_R . Furthermore, we introduce intercept i , defined as the distance from the ordinate to the intersection point of the linear fit for slope detection with the plateau value. Intercept i is a lower limit for the depletion zone. Table 1 lists the s and i values obtained for the selected deposition times. It is not surprising that intercept i , and thus the lower limit of the depletion zone, corresponds to about 150 μm and is therefore independent of the deposition time.

The existence of the depletion zone is attributed to repulsive interactions between the charged droplets during deposition. The more dominant effect, though, may originate from the rounded island shape. This geometry gives rise to a depletion

Table 1. Comparison of Slope s and Intercept i Obtained from Radial Coverage Distributions for the Deposition Times Listed

| deposition time t (s) | slope s (10^1 m^{-1}) | intercept i (μm) |
|-------------------------|-------------------------------------|---------------------------------|
| 13 | 2.1 ± 1.0 | 148 ± 24 |
| 38 | 10 ± 4 | 127 ± 46 |
| 63 | 11 ± 3 | 148 ± 37 |
| 88 | 10 ± 6 | 199 ± 46 |
| 113 | 19 ± 10 | 145 ± 20 |
| 138 | 25 ± 9 | 154 ± 18 |

zone which extends to the mean radius of the isolated PDMS islands. A depletion zone of $150 \mu\text{m}$ agrees well with the mean island radius of $74 \mu\text{m}$ present for two neighboring islands, as derived from the optical micrographs related to a deposition time of 13 s.

Figure 5 contains island size distributions deduced from optical micrographs, as shown in Figure 2a–d. The error bars correspond to the standard deviation of the frequencies received from three images per deposition time. As qualitatively recognized in Figure 2, droplet size is not uniform. We know that the ac multicone jet spray generates droplets with a range of sizes; nevertheless, the characteristic decrease from smaller to larger islands dominates island size distribution, which implies that the majority of spray droplets are relatively small and of a similar size.

During the very early stages of deposition, island density grows in a linear fashion. As deposition proceeds, the probability of island coalescence increases. Therefore, one would expect—as for atomic epitaxial systems such as Cu/Ni(100)²⁵—maximal island density, which is generally termed “saturation island density”. In fact, plotting mean island density ρ versus mean coverage θ , as illustrated in Figure 6, the

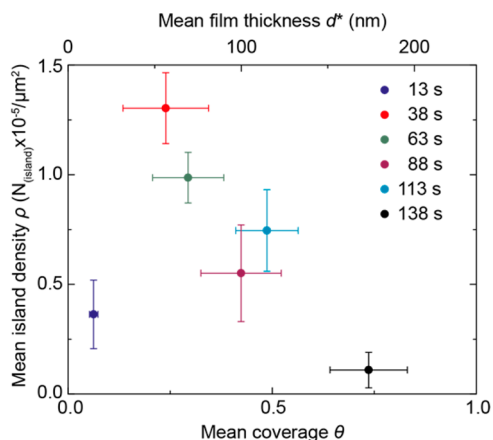


Figure 6. Mean PDMS island density versus mean coverage has a maximal value. Mean film thickness d^* is added to elucidate that for a flow rate of 267 nL/s saturation island density is reached for an average film thickness between 30 and 50 nm. The percolation threshold is found at a mean film thickness of about 150 nm.

expected maximum emerges. For representative epitaxial growth studies the maximum is observed at around 10%.^{25,26} In the present case, the maximum is found at higher coverage, presumably because of statistical growth, i.e., the absence of migrating units.

According to the two-dimensional continuum model for discs with the same radii,²⁷ the percolation threshold is reached at a coverage of 67.6%. For discs with two different radii the threshold depends on the ratio of the two radii and can be as high as 76%.²⁷ In the present case of a 5 vol % solution of DMS-V21 the percolation threshold is found above a coverage of 73.6%, as seen in Figure 6. This observation does not

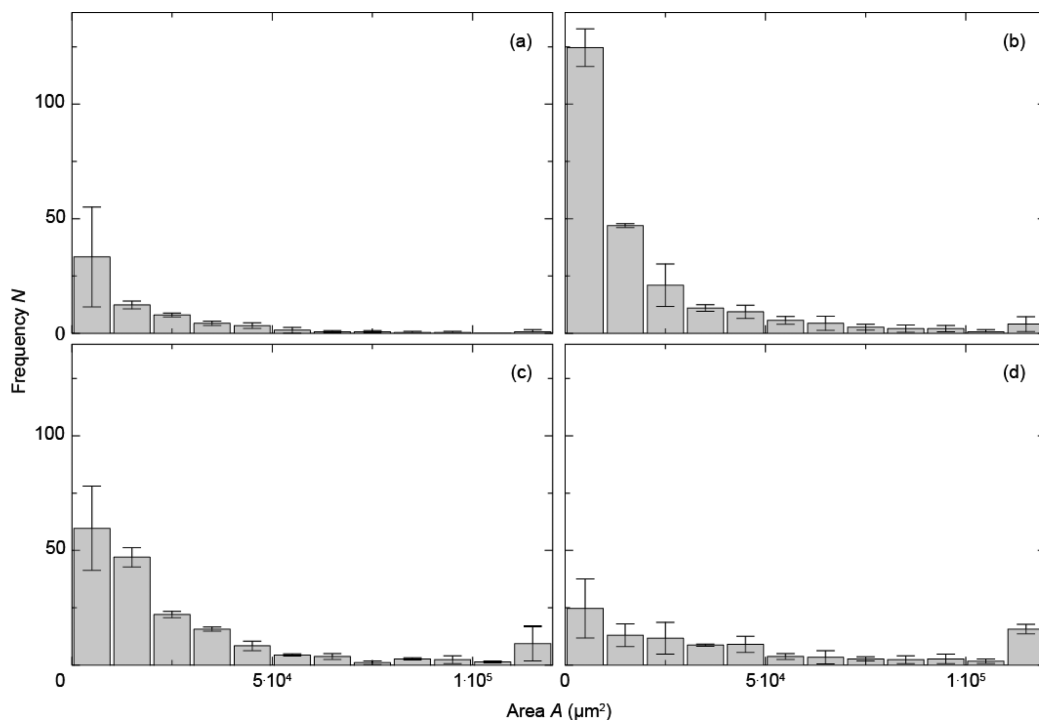


Figure 5. Abundance pattern of electro sprayed and UV-cured PDMS islands represents characteristic decay. The deposition times are (a) $t = 13$ s, (b) $t = 38$ s, (c) $t = 63$ s, and (d) $t = 88$ s.

indicate significant interactions between the droplets en route to or actually on the substrate.

Spectroscopic ellipsometry is a powerful tool for determining the surface morphology of organic films within the illuminated area.¹³ In the present study, we applied this technique to investigate PDMS films after UV curing. To this end, we employed the same experimental conditions for the deposition, i.e., 5 vol % DMS-V21 in ethyl acetate with a flow rate of 267 nL/s and spray times between 13 and 888 s.

The analysis of the experimental ellipsometry data generally requires choosing appropriate models. Here, we assume the validity of the model of nuclei growth within a squared basis, which features width w . Semispherical islands with radius R and height H constitute the UV-cured PDMS. In this model, the corners of the square base are located in the center of the PDMS island. If island size πR^2 equals the cell area of w^2 , a confluent layer is present. In a previous study,¹⁸ Ψ and Δ amplitudes damped by light scattering at the protrusions was simulated using a constant extinction coefficient of the PDMS layer with parameters for the Cauchy equation. In contrast, the nuclei growth model allows for the quantitative description of electrospayed PDMS film morphology. The overlap between model fit and experimentally measured Ψ and Δ data is quantified by the mean-square error (MSE)

$$\frac{1}{N} \sqrt{\sum_{i=1}^N \left\{ \left(\frac{\Psi_i^m - \Psi_i^{th}}{\delta\Psi} \right)^2 + \left(\frac{\Delta_i^m - \Delta_i^{th}}{\delta\Psi} \right)^2 \right\}}$$

As a baseline, ellipsometry data for the Si(100) substrate with the 2–3 nm thin, native oxide layer with parameters for the Cauchy equation were collected.

Figure 7 summarizes the data extracted from the ellipsometer measurements. For the selected deposition times t , mean island height H can be described empirically by using the linear function $H(t) = t/s \times 0.42 \pm 0.03 \text{ nm} + 25.7 \pm 6.4 \text{ nm}$ (cf. Figure 7a). Measurements taken at deposition times of 13 and 38 s reveal mean island heights of 30 ± 5 and 34 ± 5 nm, respectively. Thus, the axis offset $H_0 = 25.7 \pm 6.4 \text{ nm}$ can be interpreted as the minimal island height. This value corresponds to the mean island height measured by means of the AFM (cf. Figure 1, panels (a2) and (a3)).

The coverage shown in the diagram in Figure 7b is the ratio of the area covered by an island and the area of the square unit cell. Linear function $c(t) = t/s \times (0.0064 \pm 0.0013) - (0.0084 \pm 0.056)$ describes the increase in coverage in line with deposition time. The axis intercept related to the setup-specific delay of the spray process matches the delay extracted from the optical micrographs. The coverage extracted from the ellipsometry data corresponds reasonably well to the coverage values derived from the optical micrographs. The differences, especially high for the deposition times 88 and 138 s, are explained by the dissimilarly analyzed areas, which are 4×10 and $4 \times 4 \text{ mm}^2$, respectively.

The linear fit in the diagram in Figure 7b reveals that a spray time of $155 \pm 33 \text{ s}$ is needed to achieve 100% coverage, which is linked to a mean island height of $91 \pm 10 \text{ nm}$.

Instantaneously at spray times above 13 s, the mean island height increases above the minimal island height of about 26 nm. This effect is attributed to a stacking of droplets, and thus the electrospayed film exhibits three-dimensional growth before one single confluent layer occurs.

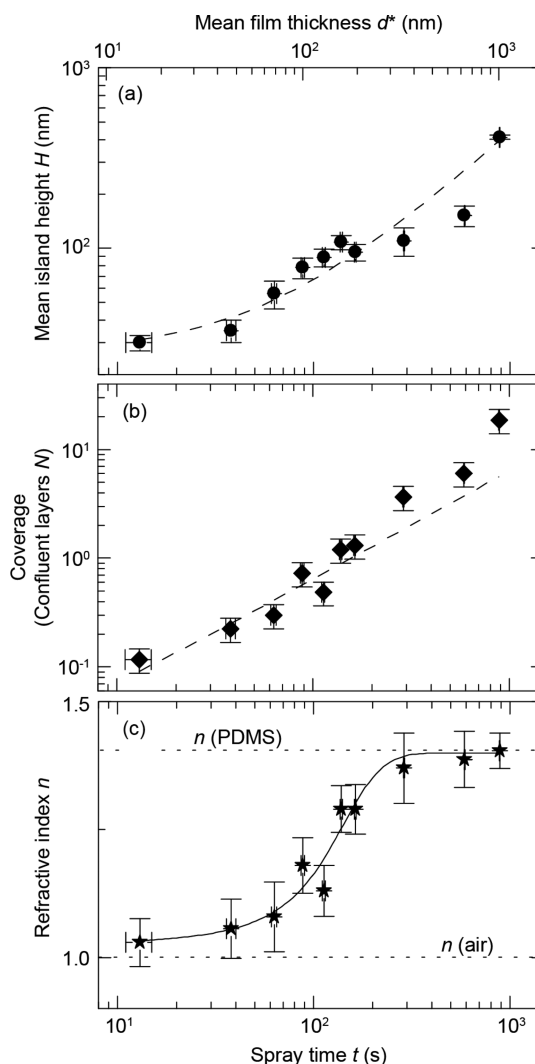


Figure 7. Morphology of the electrospayed and UV-cured PDMS depends on spray duration, as quantified using spectroscopic ellipsometry. Based on the nuclei growth model, mean island height H , diagram (a), the number of confluent PDMS layers N , diagram (b), and the refractive index n , diagram (c), are shown. The dashed lines indicate that island height $H(t)$ and coverage can be described by a linear function of the deposition time. A symmetric step function—similar to the Fermi–Dirac distribution—characterizes changes in the refractive index as the function of deposition time t , which increases from n_{Air} (632 nm) = 1 to n_{PDMS} (632 nm) = 1.396 (both values are indicated by the dotted lines).

Altering the refractive index with the deposition time given in Figure 7c's diagram supports the observation of three-dimensional growth before the confluent layer is formed. The symmetric step-like function $n(t) = 1/\exp(b(t - a) + s_1) + s_2$, with offset constants $s_1 = 2.5$, $s_2 = 1$, and fit parameters $a = (154.7 \pm 10.2) \text{ s}$, $b = (-0.0235 \pm 0.0044) \text{ s}^{-1}$, is utilized to characterize the time dependency of the refractive index between the two extrema n_{Air} (632 nm) = 1 and n_{PDMS} (632 nm) = 1.396. The inflection point at $115 \pm 11 \text{ s}$ corresponds reasonably well to the deposition time of $155 \pm 33 \text{ s}$, at which point the confluent layer forms. For this deposition time the refractive index corresponds to 1.24 ± 0.05 . This value implies the presence of air inclusions and of significant surface roughness. For deposition times above 300 s, however, the refractive index resembles that of PDMS bulk material. Thus,

we state that a compact, nanometer-thin, and smooth PDMS layer of electrospayed and cured DMS-V21 is obtained after a deposition time of 300 s. Compact and smooth films of DMS-V21 have also been compared to spin coated films in an earlier investigation for varying flow rates.¹⁸

The advantage of the proposed alternating current source with respect to a static electric field might not only relate to charge accumulation on the substrate but also particularly in the potential to prepare significantly thicker films of comparable smoothness. One might expect that the alternating current mode initially leads to comparably rough films, which heal up as the deposition proceeds.

The value of electrospaying for the economically efficient preparation of nanometer-thin polymer films is immense, as the technique is the only known alternative to MBD but allows much faster processing in sequential manner. By the use of the alternating voltage mode, one is not restricted to conductive substrates, since charge accumulation is avoided. The parameter space, however, is huge and comprises the molecular weight distribution of the starting material, the choice of the solvent and the concentration of the starting material, the geometrical arrangement of selected nozzles and substrate, and the electrical parameters, namely voltage and frequency. Therefore, much work has to be invested to exploit the method in an industrial environment.

4. CONCLUSIONS

Ac electrospay deposition and subsequent UV curing allow for fabricating submicrometer-thin, confluent elastomer films on the native oxide of a silicon wafer. For industrial-scale production, multiple nozzle arrangements should be employed, for example to manufacture large-area, multistack DEAs. Using the described experimental setup, which is a prototype for optimizing the parameters for deposition, a rather rough confluent layer about 100 nm thin is obtained. Thicker films made from the polymer DMS-V21 exhibit a smoother surface and are therefore the better choice for DEAs. As a consequence, we conclude that electrospay deposition with subsequent UV curing is an attractive, fast, and inexpensive alternative to the established techniques currently employed to produce thin PDMS films for low-voltage DEAs.

AUTHOR INFORMATION

Corresponding Author

*E-mail bert.mueller@unibas.ch (B.M.).

Funding

The authors gratefully acknowledge the financial support of the Swiss National Science Foundation (project 200021–135496) and the nanotera.ch initiative (project SmartSphincter) as well as the Swiss Nanoscience Institute (SNI) for their financial contribution to the AFM.

Notes

The authors declare no competing financial interest.

REFERENCES

- (1) Forrest, S. R. Ultrathin Organic Films Grown by Organic Molecular Beam Deposition and Related Techniques. *Chem. Rev.* **1997**, *97* (6), 1793–1896.
- (2) Johns, I. B.; Smith, J. O.; McElhill, E. A. Thermal Stability of Organic Compounds. *Ind. Eng. Chem. Prod. Res. Dev.* **1962**, *1* (1), 2–6.
- (3) Bar-Cohen, Y. Electroactive Polymers: Current Capabilities and Challenges. *Proc. SPIE* **2002**, *4695*, 1–7.

- (4) Pei, Q.; Pelrine, R.; Stanford, S.; Kornbluh, R.; Rosenthal, M. Electroelastomer Rolls and their Application for Biomimetic Walking Robots. *Synth. Met.* **2003**, *135–136*, 129–131.

- (5) Ozsecen, M. Y.; Sivak, M.; Mavroidis, C. Haptic Interfaces using Dielectric Electroactive Polymers. *Proc. SPIE* **2010**, *7647*, 764737.

- (6) Carpi, F.; Frediani, G.; Turco, S.; De Rossi, D. Bioinspired Tunable Lens with Muscle-like Electroactive Elastomers. *Adv. Funct. Mater.* **2011**, *21*, 4152–4158.

- (7) Shian, S.; Diebold, R. M.; Clarke, D. R. Tunable Lenses using Transparent Dielectric Elastomer Actuators. *Opt. Express* **2013**, *21* (7), 8669–8676.

- (8) Heydt, R.; Kornbluh, R.; Eckerle, J.; Pelrine, R. *Dielectric Elastomers as Electromechanical Transducers: Fundamentals, Materials, Devices, Models and Applications of an Emerging Electroactive Polymer Technology*; Elsevier: Oxford, 2008.

- (9) Rosenthal, M.; Bonwit, N.; Duncheon, C.; Heim, J. Applications of Dielectric Elastomer EPAM Sensors. *Proc. SPIE* **2007**, *6524*, 65241F.

- (10) Jung, K.; Kim, K. J.; Choi, H. R. A Self-sensing Dielectric Elastomer Actuator. *Sens. Actuators, A* **2008**, *143* (2), 343–351.

- (11) Töpfer, T.; Weiss, F.; Osmani, B.; Bippes, C.; Leung, V.; Müller, B. Siloxane-based Thin Films for Biomimetic Low-Voltage Dielectric Actuators. *Sens. Actuators, A* **2015**, *233*, 32–41.

- (12) Valignat, M. P.; Oshanian, G.; Villette, S.; Cazabat, A. M.; Moreau, M. Molecular Weight Dependence of Spreading Rates of Ultrathin Polymeric Films. *Phys. Rev. Lett.* **1998**, *80* (24), 5377–5380.

- (13) Lehmann, D.; Seidel, F.; Zahn, D. R. T. Thin Films with High Surface Roughness: Thickness and Dielectric Function Analysis using Spectroscopic Ellipsometry. *SpringerPlus* **2014**, *3*, 82.

- (14) Nečas, D.; Klapetek, P. Gwyddion: An Open-source Software for SPM Data Analysis. *Open Phys.* **2012**, *10* (1), 181–188.

- (15) Kroon, D.-J. Hessian Based Frangi Vesselness Filter: <http://www.mathworks.com/matlabcentral/fileexchange/24409-hessian-based-frangi-vesselness-filter>.

- (16) Tompkins, H. G.; Irene, E. A. *Handbook of Ellipsometry*; Springer-Verlag GmbH & Co. KG: Heidelberg, 2005.

- (17) Grishaev, V.; Iorio, C. S.; Dubois, F.; Amirfazli, A. Complex Drop Impact Morphology. *Langmuir* **2015**, *31* (36), 9833–9844.

- (18) Weiss, F. M.; Töpfer, T.; Osmani, B.; Deyhle, H.; Kovacs, G.; Müller, B. Electro-Spraying Nanometer-Thin Elastomer for Low Voltage Dielectric Actuators. *Adv. Electron. Mater.* **2016**, DOI: 10.1002/aelm.201500476.

- (19) Vasilets, V. N.; Kovalchuk, A. V.; Ponomarev, A. N. Photooxidation of Siloxane Polymers under Vacuum Ultraviolet Irradiation. *J. Photopolym. Sci. Technol.* **1994**, *7* (1), 165–174.

- (20) Deegan, R. D.; Bakajin, O.; Dupont, T. F.; Huber, G.; Nagel, S. R.; Witten, T. A. Capillary Flow as the Cause of Ring Stains from Dried Liquid Drops. *Nature* **1997**, *389* (6653), 827–829.

- (21) Ladegaard Larsen, A.; Sommer-Larsen, P.; Hassager, O. Some Experimental Results for the End-linked Polydimethylsiloxane Network System. *e-Polym.* **2004**, *4* (1), 548.

- (22) Voué, M.; Valignat, M. P.; Oshanian, G.; Cazabat, A. M.; De Coninck, J. Dynamics of Spreading of Liquid Microdroplets on Substrates of Increasing Surface Energies. *Langmuir* **1998**, *14* (20), 5951–5958.

- (23) Heslot, F.; Fraysse, N.; Cazabat, A. M. Molecular Layering in the Spreading of Wetting Liquid Drops. *Nature* **1989**, *338* (6217), 640–642.

- (24) Bartolo, D.; Josserand, C.; Bonn, D. Singular Jets and Bubbles in Drop Impact. *Phys. Rev. Lett.* **2006**, *96* (12), 124501.

- (25) Müller, B. Natural Formation of Nanostructures: From Fundamentals in Metal Heteroepitaxy to Applications in Optics and Biomaterials Science. *Surf. Rev. Lett.* **2001**, *8*, 169–228.

- (26) Venables, J. A.; Spiller, G. D. T.; Hanbucken, M. Nucleation and Growth of Thin Films. *Rep. Prog. Phys.* **1984**, *47* (4), 399.

- (27) Quintanilla, J. A.; Ziff, R. M. Asymmetry in the Percolation Thresholds of Fully Penetrable Disks with Two Different Radii. *Phys. Rev. E* **2007**, *76* (5), 051115.